**18th International Conference on Structural Mechanics in Reactor Technology (SMiRT 18)**
**Beijing, China, August 7-12, 2005**
**SMiRT18-C04-6**

# EXPERIMENTAL INVESTIGATION OF STRAIN, DAMAGE AND FAILURE OF HYDRIDED ZIRCALOY-4 WITH VARIOUS HYDRIDES ORIENTATIONS

**Aude RACINE**
*CEA Saclay & LMS - Ecole Polytechnique,*
*91128 PALAISEAU Cedex, FRANCE*
Phone: +33 -169333308,
Fax: +33 -169333026
E-mail: aude.racine@polytechnique.edu

**Michel BORNERT,**
**Daniel CALDEMAISON**
*LMS - Ecole Polytechnique,*
*91128 PALAISEAU Cedex, FRANCE*
Phone: +33 -169333326,
Fax: +33 -169333026
E-mail: bornert@lms.polytechnique.fr

**Claude SAINTE CATHERINE**
*CEA Saclay, LCMI, Bât 625P,*
*91191 Gif-sur-Yvette Cedex, France*
Phone: +33 -169088856,
Fax: +33 -169089324
E-mail: claude.sainte-catherine@cea.fr

**Chantal CAPPELAERE**
*CEA Saclay, LCMI, Bât 625P,*
*91191 Gif-sur-Yvette Cedex, France*
Phone: +33 -169088699,
Fax: +33 -169089324
E-mail: chantal.cappelaere@cea.fr

## ABSTRACT

This experimental investigation is devoted to the influence of the orientation of hydrides on the mechanical response of Zircaloy-4. Ring tensile tests are performed on unirradiated CWSR Zircaloy-4, charged with about 200 or 500wppm hydrogen. Hydrides are oriented either parallel ("tangential"), or perpendicular ("radial") to the circumferential tensile direction. Tangential hydrides are usually observed in cladding tubes, however, hydrides can be reoriented after cooling under stress to become radial and then trigger brittle behavior. In this investigation, we perform "macroscopic" or SEM in-situ tensile tests on smooth rings, at room temperature. We get the mechanical response of the material as a function of hydride orientation and hydrogen content and we investigate the deformation, damage and failure mechanisms. In both cases, digital image correlation techniques are used to estimate local and global strain distributions.

The results lead to the following conclusions: neither the tensile stress-strain response nor the strain modes are affected by hydrogen content or hydride orientation, but the failure modes are. Indeed, only 200wppm radial hydrides embrittle Zy-4: sample fails in the elastic domain at about 350MPa before strain bands could develop; whereas in other cases samples reach at least 750MPa before failure, with ductile or brittle mode.

**Keywords:** hydrided Zircaloy-4, orientation, failure modes, strain fields, optical methods.

## 1. INTRODUCTION

In PWR (Pressurized Water Reactors), the fuel assemblies are mainly made of zirconium alloys, because it exhibits the following properties: low neutron-absorption cross-section (this characteristic is stable under irradiation), water-corrosion resistance at in-service temperatures, microstructure stability under irradiation and satisfactory mechanical properties. However, during irradiation, these zirconium-alloy structural components are

 

oxidized by the water of the primary circuit (Zhang, 1992) according to the following equation: $Zr + 2\ H_2O \rightarrow ZrO_2 + 2\ H_2$. Part of the hydrogen produced by this reaction is picked up by the cladding tubes: the hydrogen pick-up is about 10-20% (Yvon, 2003). In service, at about 350°C, the Zircaloy-4 will take up to 125 wppm of hydrogen in solid solution (Kearns, 1967), but when for a given temperature, the solubility limit is reached, hydrogen precipitates into zirconium hydrides. Usually the density of hydrides decreases from the external to the internal layer of cladding tubes. When a bulk layer of discrete hydrides is formed along the external metallic layer, it is called a rim of hydrides and if it is only local, it is named "hydride lens".

Zirconium hydrides are known to be brittle platelets which can drastically reduce mechanical properties of Zirconium-based alloys, in particular at low temperature (less than 200°C). Two kinds of hydride-induced embrittlement exist: the first one is the delayed hydride cracking (DHC) (Northwood, 1983). This process of slow crack propagation involves the presence of hydrides at the tip of a pre-existing crack and a hydrogen diffusion process towards this highly stressed crack tip. The second one is the reduction of both the alloy ductility and the fracture toughness (Bertolino, 2003) due to the precipitation of hydrides and particularly because of a high amount of hydrogen (Grigoriev, 1996) or of a deleterious orientation of hydrides (Garde, 1996).

The changes in the mechanical response induced by hydrides (loss of ductility, reduction of fracture toughness) depend on several parameters: temperature, hydrogen content, hydride phase, morphology and spatial distribution of the hydrides and in particular their orientation with respect to the applied stress, since hydrides, because of their platelet morphology, are strongly anisotropic particles (Northwood, 1983).

This investigation is devoted to the influence of the orientation of hydrides with respect to the applied stress on strain, damage and failure mechanisms. Indeed, even if hydrides are mainly tangential (i.e. perpendicular to the radial direction of the tubes and parallel to the loading direction), because of the texture induced by the manufacturing process and then, are not noxious for usual loading conditions, they can be reoriented under some conditions of temperature and stress. For example, when discharged from the reactor, cladding tubes can experience elevated temperatures and hoop stress loading from the gas fission release and consequently, hydrides can be dissolved and then they can precipitate radially.

In the case of radial hydrides (normal to the circumferential direction of the tubes and normal the applied hoop stress), they can lead to a dramatic loss of ductility and to embrittlement of the material (Northwood (1983), Bai (1991), Racine et al. (2003)). The specificity of this work is to investigate more precisely deformation mechanisms - i.e. the distribution of stress and deformation at the microstructural level - to know if a correlation exists between the deformation modes and both the presence and the orientation of hydrides, as well as damage mechanisms at both global and local scales.

This work deals with the effects of hydride orientation on the mechanical properties of small parts of cladding tubes, i.e. smooth rings tested in tension, since these components are usually stressed in the tangential direction. In this investigation, we first perform "macroscopic" tensile tests on smooth rings, which give us the overall mechanical response of the material. Afterwards, we perform SEM in-situ tensile tests, on rings with the same geometry, in order to observe damage and failure mechanisms. In both cases, digital image correlation techniques are used to estimate global and local strain levels. Damage and failure mechanisms are observed during the SEM in-situ tests, and after all tests, failure surfaces and fracture surfaces are carefully studied. Comparisons of strain modes at the microstructural scale between hydrided and non-hydrided materials are done.

## 2. MATERIAL

### 2.1 Hydrogen charging and reorientation process

Specimens are extracted from unirradiated cladding tubes made from cold-worked stress-relieved Zircaloy-4 (annealed to 460°C during 1h30). Because of the manufacturing process (pilgrim-step cold-rolling), this material has a strongly marked texture: the majority of basal poles are 30° away from the radial direction of the tube. This texture combined with the low number of slip systems of hcp metals induces a significant anisotropy of the material.

A summary of the principal alloying elements, the microstructural and mechanical properties in the rolling direction is given in the table 1.

 

| *Alloy* | *Principal alloying elements* | *Microstructure, average grain size in the radial-tangential plane (µm)* | *Young Modulus E (GPa) @ 20°C* | *Yield Stress, $\sigma_y$ (MPa) @ 20°C* |
|---|---|---|---|---|
| Zircaloy-4, cold-worked, stress-relieved. | 0,1 w% Cr, 0,21 w% Fe, 0,31 w% Fe+Cr, 1,25 w% Sn, 1090 wppm O. | Zr α grains, small and elongated in the axial and tangential direction. | 95.3 | 670 (tension in the axial direction) ; 820 (internal pressure). |

*Table 1: Principal microstructural and mechanical characteristics of the CWSR Zircaloy-4 alloy [Data from an internal report of the CEA].*

Tubes have been hydrogen charged by a gaseous method, which was performed at 400°C in an argon-hydrogen atmosphere, up to about 200 and 500 wppm for the tests reported here. These hydrogen contents are representative of those found in in-reactor cladding tubes, respectively in the low or high grid levels. After hydrogen charging, hydrides are reoriented by heating to 400°C and then the specimens are slowly cooled under hoop stress. Stress is applied by internal oil pressure. The temperature of the reorientation process is chosen to be less than the annealing process temperature, to avoid changes in the microstructure of the metallic matrix. The cooling rate is very low in order to get the same hydride phase as the one which precipitates either in reactor (isothermal conditions) or during the storage, the δ-phase. This hydrides reorientation process does not imply plastic deformation of the tubes. The texture has also been determined by X-ray diffraction before and after reorientation treatment in order to check that no recrystallisation is induced.

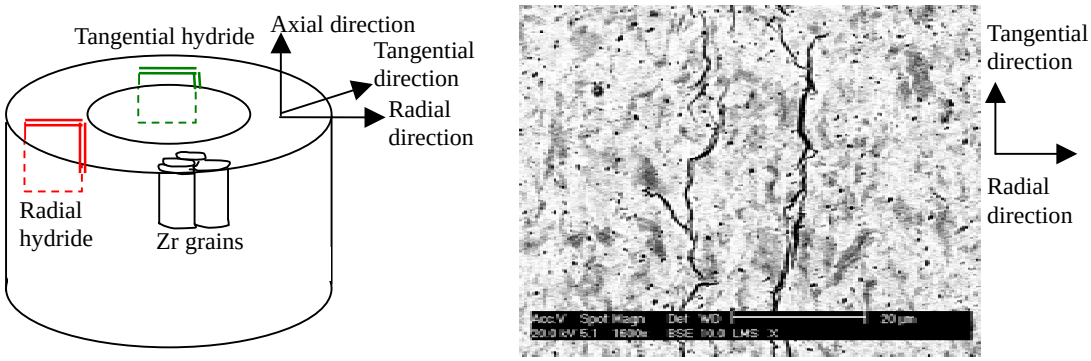


*Figure 1: Sketch of a section of a cladding tube with the different hydride orientations (left) and micrograph showing hydrides in Zy-4 at 20°C.*

Since the applied stress is tangential, hydrides which have dissolved, precipitate during cooling perpendicular to the stress applied (Marshall, 1967) and they become radial. Only about 200 wppm of hydrides can be dissolved at 400°C and reprecipitate. Depending on the stress applied, more or less hydrides precipitate "radially", it allows us to get different hydrides orientations (Figures 1 and 2): either "tangential" (parallel to the main stress direction) when no stress is applied, or "radial" (perpendicular to the main stress direction) if the stress is high, or "intermediate" (there are both tangential and radial hydrides) when the stress is less than in the previous case but more than the threshold value.

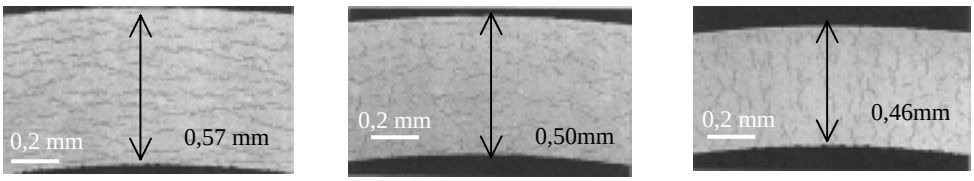


*Figure 2: Metallographic cross sections of hydrided tubes (about 230 wppm) with different main hydrides orientation: tangential (left), "intermediate" (middle) and radial hydrides (right).*

After hydridation and reorientation treatments, the ends of tubes are cut off and heated to 1250°C during 20mn: the hydrogen content of this sample is given by the quantity of gaseous hydrogen released. The hydrogen is supposed to be homogeneously distributed in the tubes. Meanwhile hydrogen content of the specimen studied here will be precisely measured at the end of this investigation (not before, because of the destructive nature of this characterization).

### 2.2 Hydrides formation

Above the solubility limit of hydrogen in zirconium, hydrogen precipitates and forms zirconium hydrides. Three phases of zirconium hydrides can form in zirconium-hydrogen system: γ, δ, ε. Their formation depends on different parameters, which are, for instance, the cooling rate and the amount of hydrogen. The hydride phase observed here is the delta phase, as revealed by X-ray diffraction, which is also the one formed in reactor. Composition of these delta-hydrides is $ZrH_x$ (x = 1.53 to 1.66).

Hydrides (delta phase) are usually described as 3D-platelets. But, different scales can be used to observe them. Whatever the scale, microscopic or macroscopic hydrides have the same crystallographic structure: the metal atoms form a face centred cubic lattice, in which the hydrogen atoms occupy tetrahedral interstitial sites. The habit plane of macroscopic hydrides is the {10-17} plane, which is 14.7° away from the basal plane. But these macroscopic hydrides are formed of microscopic hydrides, which have precipitated and are aligned themselves closely and coalesced (Chung, 2002).

### 2.3 Hydrides morphology

On cross-sections normal to the axis of the tubes (radial-tangential plane) observed under the optical microscope, one can see “macroscopic hydrides” which form thin and long bands in the section of tubes. For material hydride to 200 wppm with tangential hydrides, these bands are about 50µm apart each other. With a scanning electron microscope (SEM), the hydrides appear to be about 50 to 200µm long and 0.3 to 0.5µm wide. The segments of these macroscopic hydrides are formed of very little platelets (5 to 10µm long and 0.3µm wide). The length of the macroscopic hydrides is difficult to evaluate because they are a juxtaposition of platelets and then, the beginning and the end of a “macroscopic hydride” are not well defined. According to the literature micro-platelets are also visible with a transmission electron microscope (TEM).

Then, the observed bands in the radial-tangential plane consist of shorter hydrides, very closely aligned but slightly differently oriented. Indeed, such macroscopic hydrides cross several grains, whose orientation is mostly 30° off from the radial direction. Since the habit plane of macroscopic hydrides is about 14.7° away from the basal plane, the orientation of the platelets can vary from one grain to the next, that is why hydrides can appear like zigzag. However, in the axial-radial plane, the grains are more elongated due to the manufacturing process. Consequently, hydrides are much straighter bands.

Morphology of hydrides does not change very much with hydrogen content and hydrides orientation in the material studied. For example, in a distribution of radial hydrides with the same hydrogen content, macroscopic hydrides are shorter (50µm) and are spaced from each other in the tangential direction of about 30-60µm.
In this work, the word “hydrides” will be used to refer to the “macroscopic hydrides” (Figure 3).

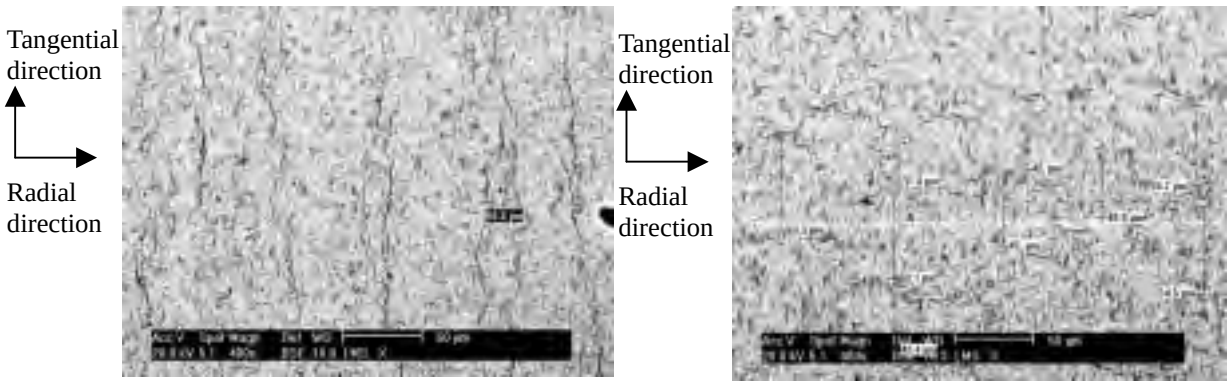


*Figure 3: Hydride distribution on the radial-tangential plane, for the average same hydrogen content (about 200 wppm) and two different main orientations, tangential (left) and radial (right).These SEM images were obtained with back-scattered electrons, and were taken at the same magnification. The interspacing distance measured in the normal direction of hydrides is indicated on the right image.*

 

### 2.4 Hydrides distribution

The first step of this investigation aimed at studying the spatial distribution of hydrides for the six different configurations of hydrided material. A qualitative evaluation through optical or SEM observations of the radial-tangential plane, let assume that at 200 wppm, the reorientation process has been very effective: the specimen with intermediate orientation contains both tangential and radial hydrides, whereas this called "with radial hydrides" contains indeed mostly radially oriented hydrides. However, for the higher content, 500 wppm, since only 200 wppm of hydrogen were likely to dissolve and to reorient, at the temperature of the reorientation process 400°C, the two reoriented configurations, called the "intermediate" and the "radial" ones, do not correspond to their names. A quantitative evaluation of the fraction of radial hydrides in each specimen has been performed. More exactly, this evaluation was done with a high resolution image for each sample, got with the SEM in back-scattered electrons, at the magnitude of x300, which is supposed to be representative of the microstructure. The proportions of length of radial hydrides have been evaluated. Hydrides have been considered as radial if they were oriented in the radial direction with +/- 45°. The orientation and the length of the particles have been evaluated with image analysis tools. In the following Table (Table 2), the proportions of length of radial hydrides are summarized for each configuration.

Since our material is hydrided with 200 or 500 wppm hydrogen and that three orientations are available for each hydrogen content: tangential (T), radial (R) or intermediate (I), we will then use following abbreviations to call the different cases: 200R for the specimen the hydrogen content of 200 wppm and the radial hydrides orientation and so on. The non-hydrided material will be designed by NH.

*Table 2: Proportion of radial hydrides in each configuration (hydrogen content and hydrides orientation) evaluated in term of hydrides length at x300 magnification.*

| ***Configuration*** | ***200T*** | ***200I*** | ***200R*** | ***500T*** | ***500I*** | ***500R*** |
|---|---|---|---|---|---|---|
| *Radial hydrides length proportion (%)* | 2.8 | 18.3 | 64.2 | 1.2 | 9.8 | 12.3 |

## 3. EXPERIMENTAL PROCEDURE

### 3.1 Specimens

For both non-hydrided and hydrided (with different hydrides orientations) specimens, tensile tests were performed, on smooth rings, whose characteristic dimensions are: thickness = 0.57mm, axial length = 5mm, external diameter = 9.5 mm (Figure 4). Smooth rings are chosen to make possible the observation of the plane faces of the rings (normal to the axial direction of the tube) during the SEM in-situ tests. All tests are carried out at room temperature.

### 3.2 Tests

Three sets of tensile tests were carried out, from which we tried to get information on strain, damage and fracture modes.

Since the hoop stress is predominant when tubes are subjected to an internal pressure or to deformation coming from the fuel pellet, we performed tensile tests on rings, even if these particular geometry and size of specimen are very restricting. For instance, it is difficult to set up an extensometer on the specimen and consequently to gain access to strain values and, it would only get us quantitative global information on the deformation, whereas we want also get qualitative and local information. Another point is that our material is heterogeneous, since it is composed of "hard particles" in a softer matrix, and we want to know how each of them deforms and if there are interaction between the both. We are also aware that the solicitation of the specimen is heterogeneous.

First, macroscopic tensile tests are done on a servo-hydraulic MTS machine, with a 100 kN load cell to get the mechanical response of the material. An extensometer is set on the rig to give us its displacement value and images are taken every 10 seconds to provide deformation of the ring instantaneously.

Then, macroscopic tensile tests are performed to investigate the global deformation modes, on electromechanical tensile machine, Instron, with a load cell of 5 kN. Specimens are tested up to fracture, at a displacement rate of 1µm/s. Load and displacement of the crosshead are recorded. Neither extensometer nor strain gage are used. The rig is tilted in order us to be able to put the two optical cameras, oriented at 90° the one from the other, to observe both the plane and the non-plane surfaces of the ring. Thanks to these "macroscopic" tests, we are able to "prepare" the SEM in-situ tests, i.e. to forecast what will be the maximal charge and where and when rupture and/or localization bands (if there are any) appear.

Eventually, SEM in-situ tensile tests are carried out. The load cell is also of 5 kN and the displacement rate is of 2µm/s, or less at the end of the test, to observe growth of damage. The plane surface is observed, but the rig can

 

be tilted to observe what happens on the non-plane surfaces. Duration of one test varies from two days to two weeks, depending on the failure mode of the specimen. In these tests attention is focused on area where fracture and localization have been observed during the macroscopic tests.

### 3.3 Experimental techniques: markers tracking and strain fields measure technique (digital image correlation)

Investigation of the global response

In order to get correct stress-strain curves, tensile tests are done with an extensometer, set on the rig, and with the markers tracking technique. But since deformation is not homogeneous in Zircaloy-4 and in particular with this geometry, it is difficult to define a macroscopic stress or strain. Nevertheless, to be able to compare all the configurations studied, and to quantify the solicitations levels, we used the values of the load normalized by the initial section. The overall deformation is characterized by the relative displacement of the north and south pole of the specimen normalized by its diameter. Then tests can be compared in terms of engineering stress-strain curves.

Investigation of the global deformation modes

To investigate more in details the global deformation modes of all these specimens, at the scale of the sample, we performed macroscopic tensile tests with optical cameras to strain maps of the specimen by using digital image correlation technique (Figure 4 and table 3).

This method allows us to characterize both the global strain (macroscopic tests generating inhomogeneous strain fields) and the local strain field (SEM in-situ tests) of a microstructure of a heterogeneous material. This technique is without contact, and then the response of the material is not disturbed. The principle is based on the comparison of two images, one of a reference and the second of a deformed configuration. By using the contrast which is (naturally or not) at the surface of the material, homologous points are automatically associated by maximizing a correlation function, computed on a neighborhood around these points. Once the positions of points are found, the displacement between the reference configuration and the deformed one is evaluated by difference and local deformations are computed by discrete derivation. This technique can be applied at different scales; it depends on optical material used and on the scale of the contrast.

In this set of tests, the non-plane area is observed with an optical camera (with a 1300 x 1030 pixels CCD) and the plane area is observed with another optical camera (with a 2048 x 2048 pixels CCD). A specklegram is deposed with an airbrush on the observed surfaces with a pattern as fine as possible (roughly 50 µm-diameter spots). One image every second is acquired all along the test. Local details on the speckled surface make identification of homologous points and then digital image correlation possible. Strain maps (gage length for local strain values of about 400µm) are plotted and allow us to characterize the macroscopic deformation modes: the principal point of interest is to know if macroscopic strain bands develop or not, and to get a better quantitative knowledge of the actual strain field in the sample, since overall displacement provide only an global value because of the complex geometry and loading mode of the test.

Investigation of the local deformation modes

Since the previous tests reveal the complexity of the macroscopic response and of the global strain fields, it is necessary to investigate the local strain fields. Consequently, we performed SEM in-situ tensile tests thanks to which we also aimed at observing damage and failure modes of hydrided Zy-4, at determining if hydrides disturb the local strain fields and what the local conditions which lead to damage are. To get quantitative information, we use as previously the digital image correlation technique, but by using microelectrolithographic technique (Figure 4 et table 3). The microstructure remains visible: correlation between the local strain levels, damage mechanisms, and the microstructure, in particular the spatial distribution of hydrides, can be investigated. Situations without hydrides, with tangential, radial or intermediate orientations of hydrides are then compared.

The methodology is the following: we observe the section perpendicular to the tube axis is observed. This surface is only mechanically polished with silicon carbide papers and oxide particles suspension: no chemical attack is performed. By this way, hydrides are not dissolved, they can be observed in the SEM with back-scattered electrons and no artefact is noticed. Indeed, in previous work (Racine, 2003), chemical etching was used and induced dissolution of hydrides and grooves in the surface at hydride platelets location. Since natural contrast is not sufficient, after polishing, 13 micro-grids are deposed by a microelectrolithographic technique (Allais, 1994). Each microgrid covers a 500µm x 500µm area.

The step of the grids is 2 µm and the width of a crossbar is only 0.3 µm. High resolution images (4096 x

 

4096 pixels) - in both secondary and back-scattered electrons - of several domains of interest are acquired for different strain levels until failure of the specimens (the domains of interest are chosen according to the observation of macroscopic tensile tests). Since it takes 15 minutes to acquire one image, the load is stopped (and slightly reduced, in order to limit relaxation during acquisition). By using the image correlation technique, local strain maps (with a gage length of 4µm) are plotted: the strain distribution can be characterized visually and isocurves indicate where the strain localizes. In addition, averages of the strain over area of about 200µm x 200µm provide the overall loading conditions under which the local deformation or damage mechanisms are activated and these averages can be compared to the local strain values measured optically during the macroscopic tests.

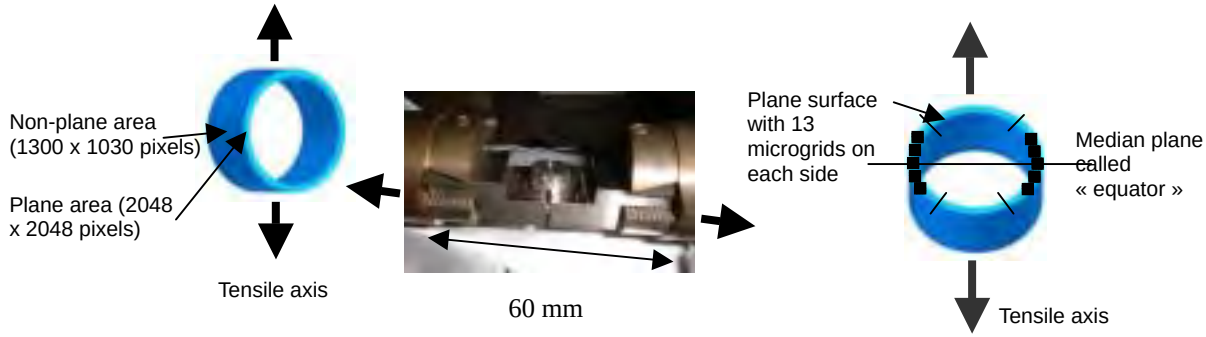


*Figure 4 : Ring tensile testing system (center); schemes of the smooth ring with the different observed surfaces for each type of tensile test ("macroscopic" on the left and SEM in-situ on the right). Arrows represent the tensile direction.*

*Table 3: Comparison of digital images acquisition means and of their respective resolution.*

| | ***Macroscopic tests*** | ***SEM in-situ tests*** |
|---|---|---|
| *Observed surface* | Non-plane and plane area | Plane area |
| *Frequency of image acquisition* | 1 image/s | Manual loading steps |
| *Image size* | 2048 x 2048 pixels and 1300 x 1030 pixels | 4096 x 4096 pixels |
| *Optical means used* | CCD optical camera | SEM |
| *Contrast* | Specklegram | Gold micro-grids |
| *Size of the observed zone* | 12 x 12 mm² and 5 x 8mm² | 300 x 300 µm² |
| *Global strain gage length* | -- | 200 – 250 µm |
| *Local strain gage length* | 400 µm | 4µm |
| *Resolution (displacement)* | $4/100^{th}$ pixel | 0.1 – 0.3 pixel |
| *Spatial resolution* | 400µm | 4µm |
| *Strain measure resolution (resolution / gage length)* | $4/100^{th}$ pixel / 40 pixels = $10^{-3}$ | 0.1 – 0.3 pixel / 40 pixels = 2.5 $10^{-3}$ to 7.5 $10^{-3}$ |

## 4. EXPERIMENTAL RESULTS

### 4.1 Global "Stress-Strain" response

In the Figure 5, engineering stress–strain curves of the seven configurations are superimposed. It is noticeable that all these curves have the same global shape. It means that the global engineering stress-strain curves exhibits the same material behaviour up to the failure points which are distributed in terms of stress and strain.

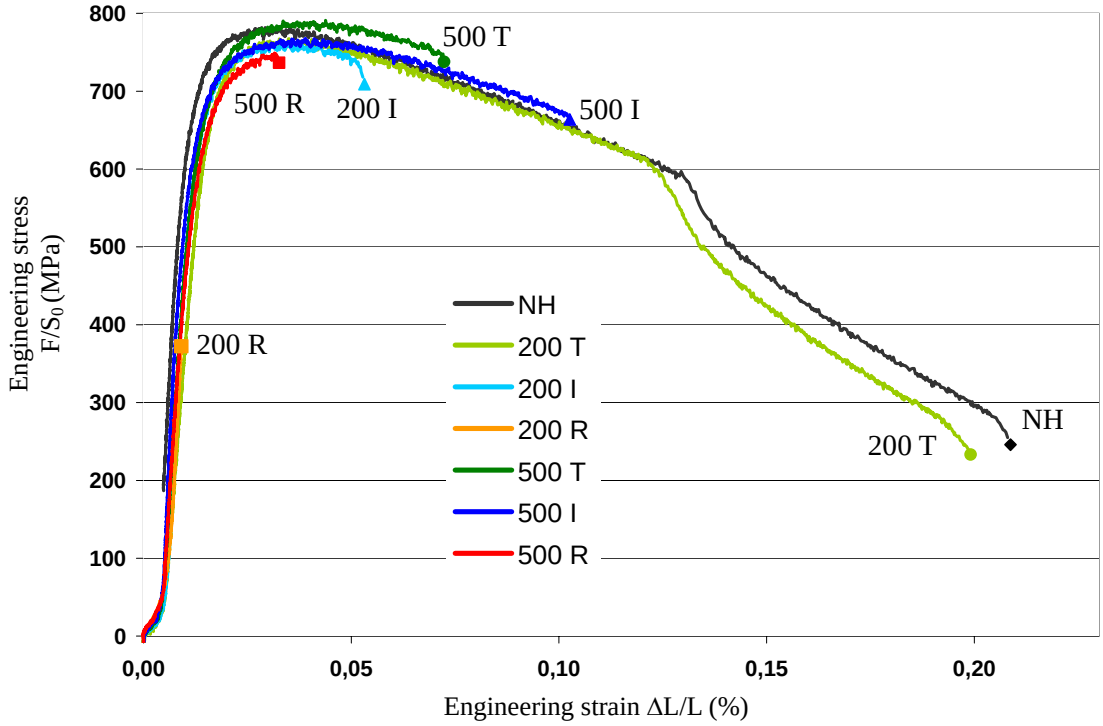


*Figure 5: "Load normalized with the initial section" – Strain curved. The strain values corresponds to the deformation measured with tracking markers technique, markers were plotted on the plane face of the ring, at the "north and the south poles".*

First, let us compare the non-hydrided case with the samples hydrided to 200 wppm. For this hydrogen content, almost all the hydrides have been dissolved during the reorientation process. Consequently, the real distributions are mainly in agreement with the names qualifying these samples.

For all these cases except the 200R, the same maximum value of "engineering stress" is reached. It is about 765 MPa. It means that necking was initiated in these samples. For the non-hydrided specimen, final fracture occurs later than for the other specimens. The global response is ductile. For the 200T case, the curve is almost the same: the failure strain is slightly but not significantly smaller (1 %). The response is almost the same, with in particular the same final failure scheme.

In the 200R specimen, the response is very different from the first two cases: while the first linear elastic part of the load-displacement curve is almost the same, the fracture happens suddenly (between 300 and 370 MPa), without prior development of plasticity and the crack propagates along a straight line, normal to the applied load. For the 200I specimen with the same hydrogen content and with "intermediate" hydrides, the maximal load normalized by the section is almost the same as without hydrides, plasticity mechanisms are of the same kind, but the fracture mode is totally different: final fracture occurred along a straight line, normal to the applied load, it seems to be brittle like in the case with radial hydrides. For the hydrogen content of 200 wppm, the three cases are very different from each others for the failure point but similar for the stress-strain macroscopic curve.

Then, let us consider the three last cases which contain about 500 wppm hydrogen. The three curves are a lot closer ones each others than those for the 200X cases. Indeed, the maximal value of the force normalized by the section is once again almost the same. The curve of the 500R case reaches the maximal value and then fails, whereas the 500I and 500T cases go further, but fail suddenly, along a straight line normal to the applied load, for a strain value which varies from one experiment to the other. For instance, in the curves of the Figure 5; the 500T case (failure strain is about 7%) is less ductile than the 500I one (failure strain is about 10%), whereas in former tests, 500T was more ductile than 500I.

During the SEM in-situ tensile tests, we get Engineering stress-strain curves which are similar, except that the values of maximal "engineering stress" are more scattered. This could be due to the multiple interruptions of these tests, during which the material relaxes more or less.

*Table 4: Average of principal values got with the two sets of macroscopic tests (these with optical camera and those with markers tracking).*

| ***Main orientation hydrides*** | ***Average hydrogen content (wppm)*** | ***Maximal load normalized by initial section (MPa)*** | ***Load at rupture normalized by initial section (MPa)*** | ***Elongation at rupture (%)*** | ***Failure mode*** | ***Existence of necking?*** |
|---|---|---|---|---|---|---|
| | Non-hydrided | 770 | 316 | 21 | Ductile shear | Yes |
| *Tangential* | 220 | 758 | 316 | 20 | Ductile shear | Yes |
| *Intermediate* | 228 | 771 | 713 | 5,3 | Brittle with ductility. | A small one |
| *Radial* | 243 | 336 | 336 | 0,9 | Totally brittle | Not at all |
| *Tangential* | 500 | 784 | 715 | 7,2 | Brittle with ductility. | A small one |
| *Intermediate* | 561 | 773 | 701 | 10,3 | Brittle with ductility. | A small one |
| *Radial* | 558 | 740 | 712 | 3,3 | Brittle with ductility. | A small one |

### 4.2 Global deformation and failure modes

Thanks to correlation technique we get strain maps (Figure 6), as described previously. Strain maps given by the image correlation technique can be linked with the "stress-strain" curves, in order to gain access to the local deformation modes for different stress levels. From macroscopic tests, we obtain maps of the non-plane areas, which cover about 5 x 7mm and represent the local strain values. As previously discussed, the strain gage length for these maps is about 400µm. Those of the plane area, also issued of the macroscopic tests cover a larger area, from about 12 x 12 mm. With these two series of maps, we determine if macroscopic strain bands develop. In the same way but at another scale, SEM in-situ tests give us strain maps of the microstructure of small parts (300 x 300 µm²) of the plane area, and we can determine if microstructural strain bands appear or not, and whether they are correlated with the presence of hydrides.

We used the information given by theses maps, and those issued from the post-mortem fracture surface observation to gather the seven cases into three damage and failure modes.

*Ductile mode: NH, 200T*

Firstly, let us describe why NH and 200T cases belong to the "ductile mode" family. For these two specimens, the global response is ductile, macroscopic strain bands oriented with about 50° with respect to the tensile axis develop and necking occurs through the thickness. Final fracture occurs along these macroscopic strain bands.

Localization bands appear at the maximum stress and macroscopic initiation of ductile failure occurs at the intersection of these two shearing bands. The very abrupt change of slope in the last part of σ-ε curves coincides with the initiation of such a "cavity" at the intersection of these bands. The cavity grows up leading to the final failure of the sample. Thus the tangential hydrides at this content do not change the global behaviour of Zircaloy-4.

However, failure fracture surface are different: in NH material, three zones are distinguishable: at the centre, where the cavity appeared at the intersection of macroscopic bands, specimen exhibits ductile fracture surface, with microvoids coalescence. A little away from the central area, the fracture surface is plane, because of shearing occurring in the macroscopic bands. And close to the plane surface where the bands appear, it is once again ductile with dimples.

For the 200T material, the so-called "secondary cracks" (Huang, 1994), that is to say long cracks, whose dimensions are close to those of hydrides in the radial-axial plane, and which probably correspond to hydrides can be observed on the fracture surface. Either these hydrides broke along the tangential-axial plane, or there was decohesion between the hydride and the matrix interface. Elsewhere, between these secondary cracks, surface is covered by microvoids. Most of these secondary cracks are long (200 to 300 µm) and relatively thin (about 20 µm).

 

*Purely brittle mode: 200R*

Secondly, let us see the second and the third families. The common point of all these specimens (i.e. 200I, 200R, 500T, 500I, 500R) is the final fracture: final fracture occurred along a straight line, normal to the applied load. But some differences must be described.

In the 200R specimen, the response is very different from the other cases: while the first part of the σ-ε curve is almost the same, the fracture happens suddenly (between 300 and 370 MPa), without prior development of plasticity and the crack propagates straightaway, normally to the applied load.

The strain map just before final failure confirms that the rupture is brittle: no significant deformation can be noticed, the deformation heterogeneities must be due to the test itself: indeed at the beginning the ring is mostly submitted to bending and not to pure tension. Besides, the images from which correlation is done are plane projections of a non-plane area and motion: artefacts are induced and especially visible for such low strain levels.

The fracture occurred in the median plane of the specimen and propagated along radial hydrides which were more or less aligned along a radius of the ring, in a domain where the stress is normal to the direction of this radius.

Fracture surface is totally free of microvoids. It exhibits “steps” of flat brittle regions, which are likely to reflect the size of hydride platelets. Indeed, these steps are observed in the radial-axial plane, in which radial hydrides have precipitated.

*Brittle mode after ductile deformation: 200I, 500T, 500I, 500R*

For the 200I specimen, macroscopic strain bands and necking are observed at the same positions as in NH or 200T cases, but the fracture mode is brittle, like in the 200R case. The fracture surface confirms and explains this double nature. In the centre of the non-plane area, at the intersection of macroscopic shear bands, plasticity developed: the corresponding surface rupture is curved (as if a cavity was initiated at the intersection of shear bands) and exhibits microvoids and small secondary cracks (about 50 µm) on about 500 x 500 µm². But elsewhere “steps” of flat surfaces, which are mainly brittle are noticeable and remind the brittle fracture surface of 200R.

The 500 cases are very similar to each others, except that necking is noticeable almost only for 500T. Macroscopic shear bands develop, but the final failure is sudden and normal to the applied load independently of the macroscopic shear bands. Differences between the failure surfaces are not easily noticeable: in 500R and 500I cases, there are a lot of secondary cracks, and a lot of steps of flat brittle regions. Secondary cracks are shorter than in the 200T case: about 50µm long, but they are much more numerous. Steps are elongated in the axial direction, but their dimensions are not easy to evaluate: their length is less than 100µm and their spacing in the transverse direction is about 40µm. On the surface of 500T, steps are more elongated (15µm thick and from 30 to 100µm long) and more ductile zones are noticeable.

Then, we assume that the secondary cracks correspond to former tangential hydrides, large flat regions to radial hydrides platelets, and thin flat regions to clusters of tangential hydrides.

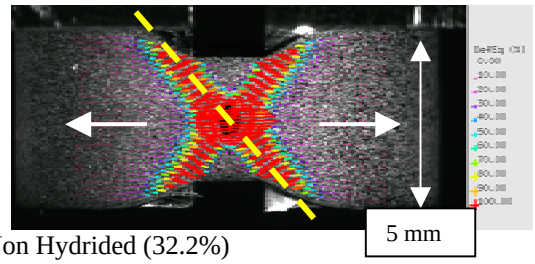


Non Hydrided (32.2%)

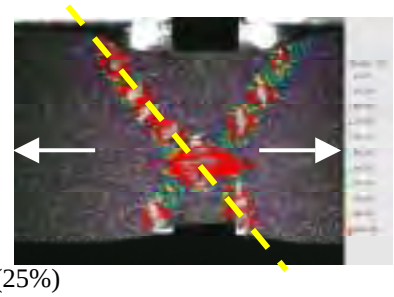

200T (25%)

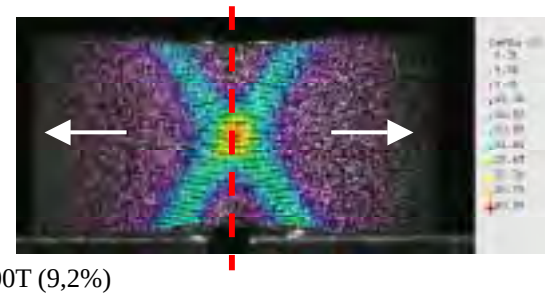

500T (9,2%)

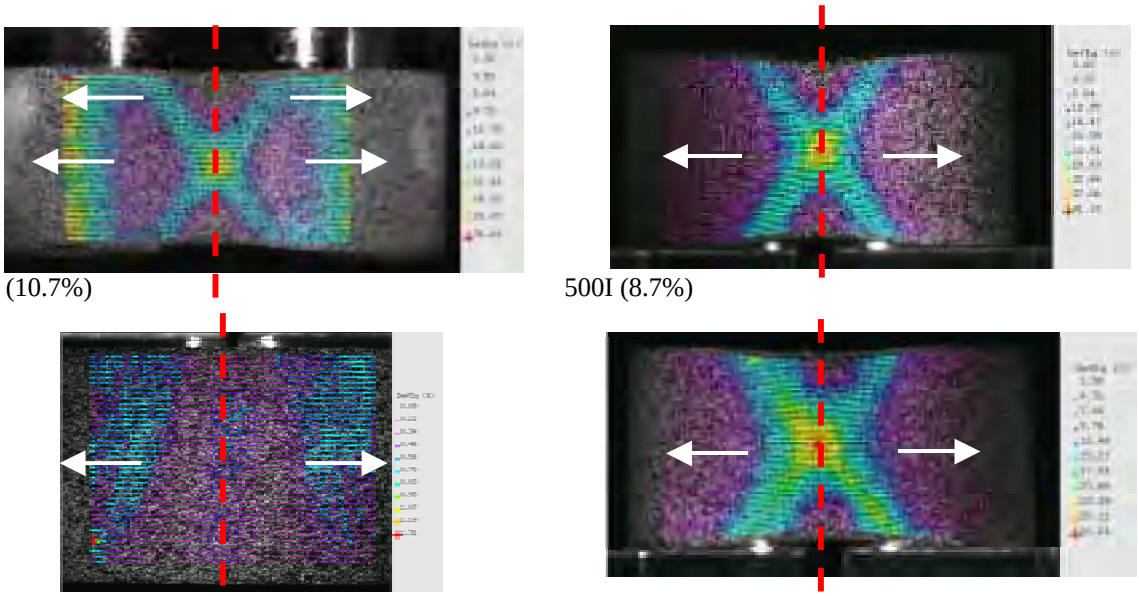


*Figure 6: Strain maps before failure of the different materials studied, represented in the deformed configuration. The covered area is of about 5 x 7 mm². The maximal deviatoric strain value is given by the red color. Between parenthesis is indicated the value of the average strain in the tensile direction, which is computed over the contour domain. The arrows represent the tensile axis and the dotted line the final crack path. These maps are a qualitative and quantitative means to investigate strain localization modes during deformation.*

### 4.3 Local deformation modes and damage micromechanisms

First, thanks to the digital image correlation technique, we get the averaged strain value on different domains corresponding to a part of a micro-grid which has been deposed on the plane surface. For each specimen, about 13 micro-grids are deposed on the left part and the right part of the ring with respect to the tensile axis. The size of the domains studied varies, because it depends on the quality of the grids. But generally, they cover a 250 x 250 µm² area. The average strain values are very different from one domain to another, because of the macroscopic heterogeneity of the strain field: the solicitation is of course not pure and does not correspond only to pure tension. At the beginning of tests, right and left parts of the rings become straighter and are mostly submitted to bending. Then, they undergo tensile loading. However, in all cases, the strain values are the most significant where the macroscopic shear bands - which develop on the non-plane area – appear on the plane area. For instance, the average strains (strain in the tensile direction) in the most deformed domains are the following: NH: 30%, 200T: 39%, 200I: 24%, 200R: 2%, 500T: 21.6%, 500I: 7.5%, 500R: 2.4%. These values cannot be directly compared, because the areas investigated are not located exactly in the same way and they do not cover the same surface.

Strain maps (relative to a 4µm gage length) represented by isovalues curves are superimposed on the microstructure images in order to observe whether strain heterogeneities are linked or not with the presence of hydrides. In all cases, except the 200R, strain localizes in microbands at the microstructural scale. The spatial distribution of microbands is almost the same from one case to the other, but there are more numerous in the NH case. Besides, microbands are present only in the zones where the strain values (average value on a domain) are the highest (i.e. where the macroscopic shear bands appear on the plane area

To know if hydrides affect the local plastic flow, a more detailed statistical analysis is required and currently under progress in order to be able to draw more quantitative conclusions about the role of hydrides on deformation mechanisms; in particular, these microscopic strain bands and their statistical properties are compared in different cases. We get histograms of local equivalent strains normalized with respect to the overall equivalent strain on the investigated area: on the x-axis, is reported the equivalent strain (1 corresponds to the normalized equivalent strain, 2 corresponds to the double of the normalized equivalent strain …), and on the

 

y-axis, its probability. These histograms have been drawn and superimposed only in three cases: NH, 200T and 200I, for several deformation levels and for the most deformed zone of each specimen. All these curves are superimposed but two groups are distinguishable: the first one gathers almost all the cases, curves are symmetrical with respect to the normalized equivalent strain value, they corresponds to the first steps of deformation (NH, 200T) or to moderate values of average strain (200I); the second group of curves is slightly shifted to the left, it concerns the 200T and NH cases at the last steps of deformation, and the dissymmetry of curves reflects the strain localization at the macroscopic level.
Then, since all the curves, whatever the case, hydrided or not, are superimposed, it would lead us to conclude that the level of heterogeneity of microstructural deformation does not seem to be significantly disturbed by hydrides.

Besides giving qualitative and quantitative information on local strain modes, SEM in-situ tests are used to observe damage and fracture micro-mechanisms (Figure 7).
For NH and 200T cases, since shear failure occurs along one of the macroscopic shear bands, damage is mostly noticeable where theses bands appear on the surface. In the last steps of deformation, surfaces in these domains are much damaged, but there are very few cavities in hydrides. It is difficult to assert as others authors (Arsène, 1997) that hydrides have deformed or have rotated, because the surface is so changed, there is so much relief and also contrast, that hydrides are difficult to detect.

For 200R, failure occurs suddenly and without prior deformation, and crack propagated via a path trough hydrides, which can be deduced by the comparison between the images of the initial and final states. The final crack is normal to the applied load and occurs in the zone called “equator”, unlike the previous cases. But we are unable to say if hydrides crack themselves in their thickness or if there was a separation between the hydride-matrix interface, contrary to (Coleman and Hardié, 1966) who assert the first hypothesis is true.

The 200M case undergoes damage in surface at the same location as 200T and NH, and no cavity is noticed, but the final failure lies normal to the applied load, as explained previously.

All the 500 cases are the most interesting from the point of view of damage, because, only in these cases, we really see “damage” on the plane surface, i.e. cavities in hydrides. Indeed, in an about 500 x 500 µm² zone centred on the failure, hydrides (which are mostly tangential, as explained previously) are broken in several parts and several cavities, as large as hydrides thickness, are present along hydrides. Their size is variable, it depends on hydride thickness and of closeness of failure. But, these cavities must form just before final failure, and since this is very sudden, we were able to observe cavities only once the specimen failed.

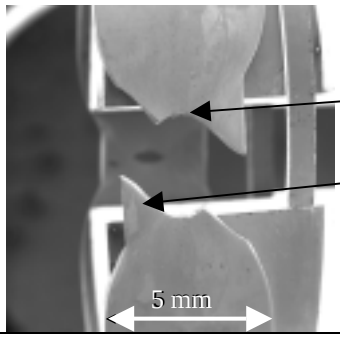


NH: overall view of the necked specimen, and the shear failure through the central cavity.

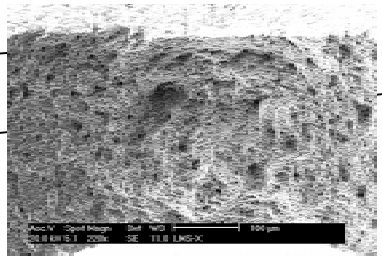

Very ductile surface failure, at the center of the specimen, with microvoids.

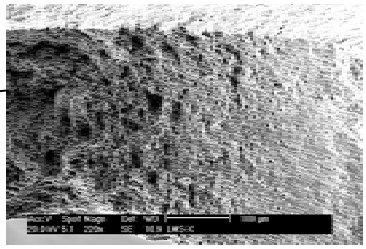

Transition area of the surface failure, with a shearing zone.

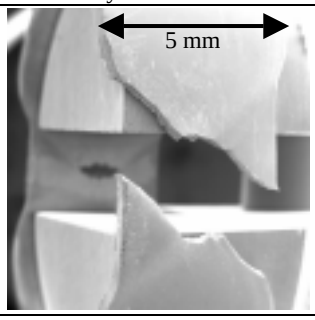


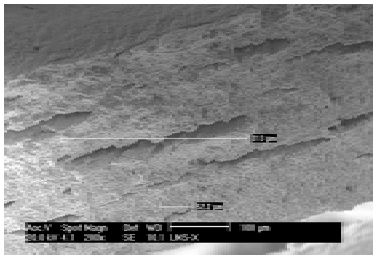

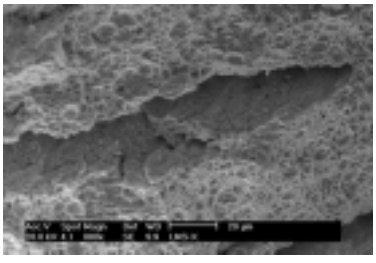

| | | |
|---|---|---|
| 200T: overall view: necking, shear bands and central cavities on each side. | Ductile surface failure with very long secondary cracks. | Zoom on a secondary crack. |
| 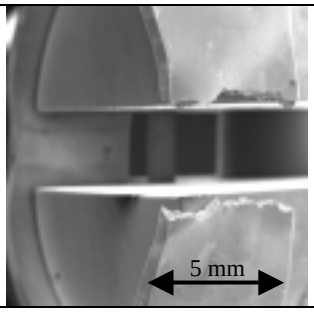 | 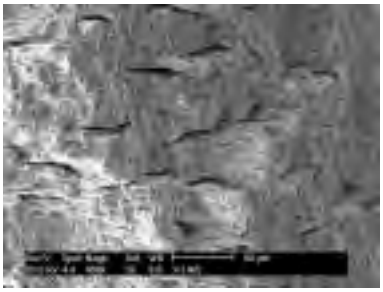 | 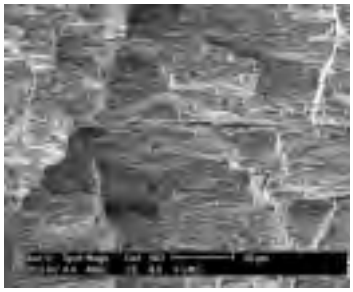 |
| 200I: overall view. Unlike previous cases, failure is normal to the applied load, but shear bands are visible. | At the center of the surface failure: ductility with microvoids and secondary cracks. | From each side of the center: brittle surface failure with “steps”. |
| 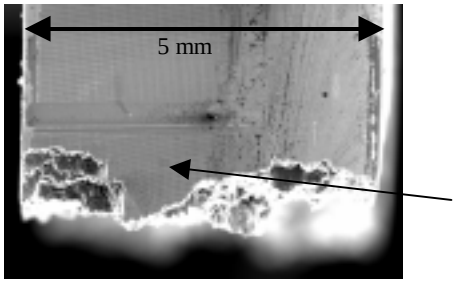 | 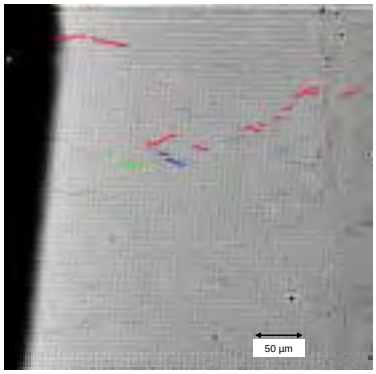 | 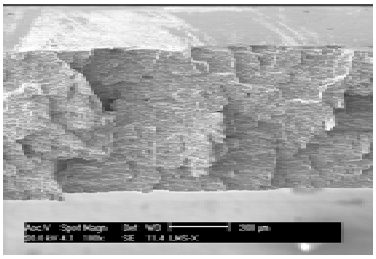 |
| 200R: Part of the ring just above the failure. | Path of radial hydrides through which the final crack propagated. | Surface failure with “steps” of flat brittle regions. |
| 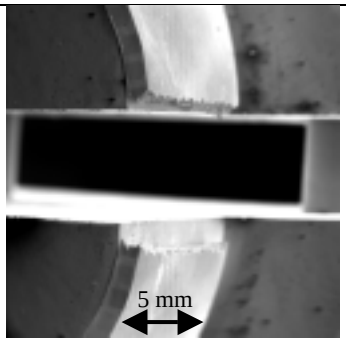 | 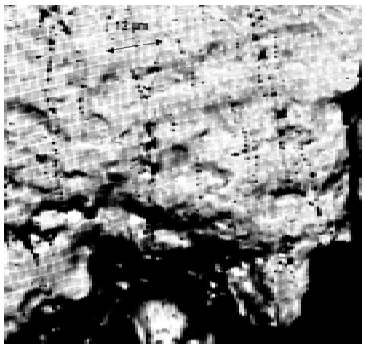 | 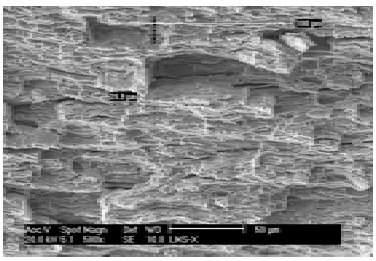 |
| 500T : Overall View | Plane surface after failure : cavities in hydrides | Surface failure |
| 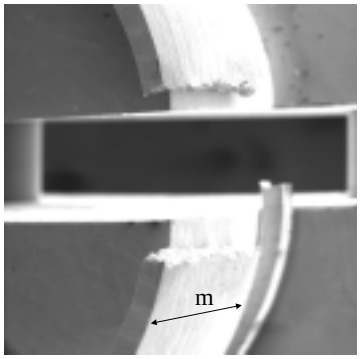 | 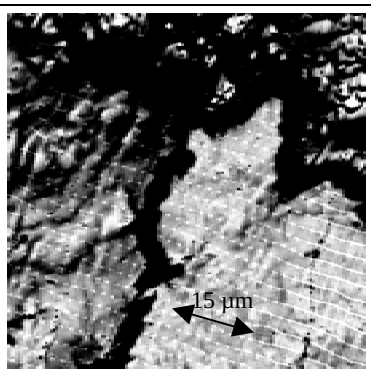 | 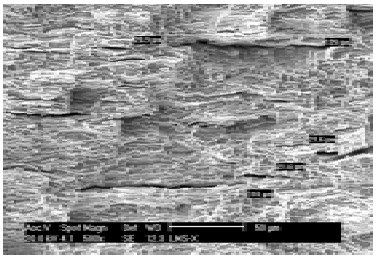 |
| 500I : Overall view | Plane surface after failure : cavities in | Surface failure with “steps” and |

| | | |
|---|---|---|
| | hydrides | small secondary cracks |
| 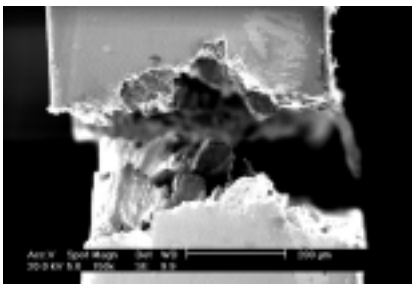 | 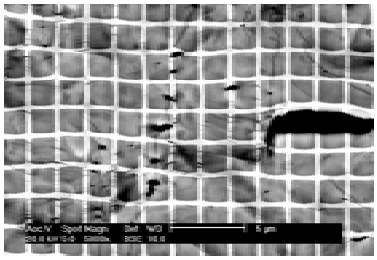 | 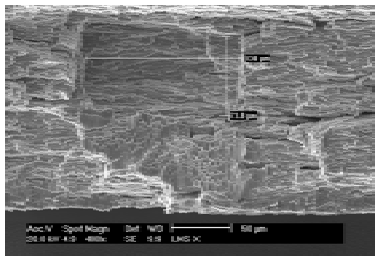 |
| 500R Plane surface after failure | Plane surface after failure : cavities in hydrides | Surface failure with “steps” |

*Figure 7: Images of specimens showing the damage and failure mechanisms (overall views and fracture surfaces).*

## 5. DISCUSSION

### 5.1 Mechanical response

In accordance with results got previously by (Marshall and Louthan, 1963), the results of these tensile tests on smooth rings show that:

- Hydrogen content does not change yield tensile stress, maximal stress, and more generally the shape of the mechanical response; only the ductility is reduced when the hydrogen content increases.
- The most significant parameter which drastically decreases hydrided Zircaloy-4 ductility is the orientation of hydrides platelets with respect to the applied stress. Indeed, even if the hydrogen content is relatively low, specimens exhibit no macroscopic ductility at all, even at 200 wppm, if the hydride orientation is markedly perpendicular to the applied stress.

### 5.2 Initiation and propagation of failure

Three cases are distinguishable:

- First, the non-hydrided material is ductile. Low hydrogen content (about 200 wppm) and tangential hydrides do not change this failure mode, only failure surfaces are different. Ductile failure occurs by shearing. The most deformed areas of the plane surface, where macroscopic shear bands appear, do not exhibit microvoids in hydrides: this is likely due to the shear phenomenon, and to the geometry of the specimen, which prevents microvoids to nucleate and growth where the strain values are the highest.
- Second, materials hydrided with higher hydrogen content (about 500 wppm), but with mostly tangential hydrides (whatever the name “tangential”, “intermediate” or “radial”) develop macroscopic shear bands as well. However, the mechanisms of failure propagation are different: because the lower plastic elongation with respect to the previous case, the shearing does not develop, and the fracture propagates normal to the applied tension. But, since the fracture appears in the equator area, in a zone in a pure tension, cavities appear in hydrides located in this area.
- Third, materials with 200 wppm of either radial or intermediate hydrides fail in a brittle way. In the first case, plasticity has no time to develop at all, and the final crack path is identified to occur along the hydride length; in the second one, plasticity is initiated, but not propagated, because of the presence of some radial brittle hydrides oriented normal to the applied stress, which tend to turn the failure propagation in an instable one.

### 5.3 Micro-scale deformation modes

According to both strain maps superimposed of the microstructure and histograms of deformations, it seems that the presence of hydrides does not affect significantly the distribution of microscopic strain bands.

## 6. CONCLUSIONS

In this investigation, tensile tests on smooth rings were performed, on Zircaloy-4, non-hydrided, or hydrided to 200 wppm and 500 wppm. For each hydrogen content, hydrides were reoriented under stress of different levels at 400°C, in order to get several distributions of hydrides orientations: tangential (no stress reorientation), intermediate or radial. In fact, the distributions of hydrides are really different only for the lower hydrogen

 

content. For the higher hydrogen content, the distribution of hydrides is mainly tangential, because of hydrogen solubility limit consideration.

Among the seven studied configurations, specimens exhibit few differences concerning deformation modes, but more on rupture initiation and propagation. The basis scheme, which occurs for non-hydrided material and 200T, is the development of macroscopic shearing bands, at the intersection of which failure is initiated and along which it propagates. When the hydrogen content is higher but the main hydride orientation is still parallel to the applied stress, the failure will appear earlier: the bands have been developed but the final rupture does not occur by shearing, it will propagate normally to the applied load. Eventually, if the hydrogen content is low but if hydrides are radial, failure will be totally brittle (200R), and if there are both radial and tangential hydrides (200I), initiation of failure occurs at the intersection of the macroscopic bands, but it will propagate as in the brittle case.

The modelling of this particular heterogeneous material behaviour is under way with a damage approach taking into account the anisotropic distribution nature of the hydrides and their orientation.

## REFERENCES


Allais L. et al., (1994), Acta metallurgica and materalia, Vol. 42 (11), pp. 3865-3880.
Arsène S., (1997), Ph-D Thesis.
Bai J., (1991), Ph-D Thesis.
Bertolino G., Meyer G., Perez Ipina J., (2003), Journal of Nuclear Materials, Vol. 320, pp. 272-279.
Chung H.M., Daum R.S., Hiller J.M., Billone M.C., (2002), Proceedings of the ASTM Conference on Zirconium in the Nuclear Industry, ASTM STP 1423.
Coleman C.E., Hardié D., (1966), Journal of Less Common Metals, Vol.11, pp. 168-185.
Doumalin P., (2000), Ph-D Thesis.
Garde A.M., Smith G.P., Pirek R.C., (1996), Proceedings of the ASTM Conference on Zirconium in the Nuclear Industry, ASTM STP 1295.
Grange M., (1998), Ph-D Thesis.
Grigoriev V., Josefsson B., Rosberg B., (1996), Proceedings of the ASTM Conference on Zirconium in the Nuclear Industry, ASTM STP 1295.
Huang J.H., Huang S.P., (1993), Journal of Nuclear Materials, Vol. 208, pp. 166-179.
Kearns J.J., (1967), Journal of Nuclear Materials, Vol. 22, pp. 292-303.
Marshall R.P., (1963), Journal of Nuclear Materials, Vol. 244, pp. 49-59.
Marshall R.P., Louthan M.R. Jr, (1963), Transactions of the ASM, Vol. 56, pp. 693-700.
Northwood D.O., Kosasih U., (1983), International Metal reviews, Vol. 28, n°2, pp. 92-121.
Racine A. et al., (2003), J. Phys. IV France, Vol. 106, pp. 109-118.
Yvon P., Lemaignan C., (2003), J. Phys. IV France, Vol. 106, pp 185-193.
Zhang J.H., (1992), Ph-D Thesis.



**Acknowledgments:** The theme of this study is based on PRECCI and PROMETRA projects which are performed by CEA either with EDF, Framatome-ANP or with IRSN. The support from those projects and organisations is here greatly acknowledged.